J Nanopart Res (2011) 13:7075–7083
DOI 10.1007/s11051-011-0620-8

RESEARCH PAPER

Structural and catalytic properties of ZnO and Al_2O_3 nanostructures loaded with metal nanoparticles

Osama A. Fouad · Abd El Rahman S. Khder · Qilin Dai · M. Samy El-Shall

Received: 20 June 2011 / Accepted: 20 October 2011 / Published online: 5 November 2011

Abstract Nanostructured zinc oxide (ZnO) nanobelts and aluminum oxide (Al_2O_3) nanoribbons have been grown successfully from the vapor phase. XRD results confirmed the purity and the high quality of the formed crystalline materials. TEM images showed that ZnO nanostructures grew in the commonly known tetrapod structure with nanobelts separated from the tetrapods with an average width range of 10–30 nm and a length of about 500 nm. Al_2O_3 nanostructures grew in the form of nanoribbons with an average width range of 20–30 nm and a length of up to 1 μm. The catalytic oxidation of CO gas into CO_2 gas over the synthesized nanostructures is also reported. Higher catalytic activity was observed for Pd nanoparticles loaded on the ZnO nanobelts (100% conversion at 270 °C) and Al_2O_3 nanoribbons (100% conversion at 250 °C). The catalytic activity increased in the order Cu < Co < Au < Pd for the metal-loaded nanostructures. The preparation methods could be applied for the synthesis of novel nanostructures of various materials with novel properties resulting from the different shapes and morphologies.

Keywords ZnO nanobelts · Al_2O_3 nanoribbons · Metal nanoparticles · Catalytic oxidation of CO · Supported nanoparticle catalysts

O. A. Fouad
Central Metallurgical Research and Development Institute (CMRDI), P.O. Box 87, Helwan, Cairo 11421, Egypt

O. A. Fouad (✉) · A. E. R. S. Khder · Q. Dai · M. S. El-Shall (✉)
Department of Chemistry, Virginia Commonwealth University, Richmond, VA 23284-2006, USA
e-mail: oafouad@yahoo.com

M. S. El-Shall
e-mail: mselshal@vcu.edu

Q. Dai
e-mail: qlai2008@yahoo.com

A. E. R. S. Khder
Department of Chemistry, Mansoura University, Mansoura, Egypt
e-mail: askhder2244@yahoo.com

Introduction

The growth of semiconductor nanostructures has been demonstrated by various methodologies, including the vapor–liquid–solid (VLS) growth (Wu and Yang 2000; Peng et al. 2002) oxide-assisted growth (Chen and Yeh 2000), template-assisted growth (Bai et al. 1999), vapor-phase transport (Wu and Yang 2000; Peng et al. 2002; Chen and Yeh 2000; Bai et al. 1999), chemical vapor deposition (Yazawa et al. 1992), arc discharge (Choi et al. 2000), laser ablation (Duan et al. 2000), solution growth (Holmes et al. 2000), and a template-based growth method (Huang et al. 2000; Li et al. 2000). A novel approach to the fabrication and manipulation of nanostructured materials is crucial to

the execution of nanotechnology in many vital industrial applications such as catalysis (Aoki et al. 2000). Vapor growth of nanostructured materials is a promising process for the fabrication of the materials in pure and high quality crystalline forms. It is a simple and relatively low-cost process.

Most of the studies in heterogeneous catalysis involve the use of spherical nanoparticles or nanoparticles of undefined shapes as catalysts (Somorjai 1994; Moser 1996; Chusuei et al. 2001; Henrich and Cox 1996; Ying and Tschope 1996). However, recent studies have investigated the effects of the nanoparticles' shape on the activation energy and the rates of the catalytic reaction (Narayanan and El-Sayed 2004, 2005; Huang et al. 2005; Glaspell et al. 2005, 2006a, b). The effect of particle shape on the catalytic activity depends on the density of the surface active sites (Narayanan and El-Sayed 2004, 2005; Huang et al. 2005; Glaspell et al. 2005, 2006a, b). Thus, metal nanoparticle catalysts with defined sizes and shapes may exhibit different activities when supported on metal oxides having different shapes. The high surface-to-volume ratio of the one-dimensional (1D) nanostructured semiconducting materials such as nanobelts, nanoribbons, nanorods, nanowires, and nanotubes could lead to remarkable chemical and physical properties which provide an advantage of using such structures as high surface area supports in catalysis. The large number of surface and edge atoms provides active sites for catalyzing surface based reactions. Recent approaches have utilized carbon nanotubes as supporting materials for the dispersion and assembly of metal nanoparticle catalysts such as Au and Pt (Mu et al. 2005; Kongkanand et al. 2006). The increase in the catalytic efficiencies has been attributed to the increased surface areas and the well-dispersed catalyst on the carbon support (Kongkanand et al. 2006).

Among many semiconducting materials, ZnO has been extensively investigated as a promising candidate for various optoelectronic device applications. Zinc oxide is one of the most common semiconductor materials applied to produce the devices that use surface acoustic waves, elements of integrated optics, gas sensors, and solar cells. In addition, further applications are expected in other areas such as catalysis in the form of one-dimensional nanowires (Wu and Yang 2000; Peng et al. 2002). One-dimensional single-crystalline ZnO nanostructures have been synthesized successfully by many research groups (Huang et al. 2000; Li et al. 2000; Aoki et al. 2000). ZnO nanobelts were synthesized at 900–1350 °C by thermal evaporation of Zn and ZnO powders (Fouad et al. 2008, 2010, 2006; Lee et al. 2004; Li et al. 2001). In addition, catalyst and catalyst-free wire growth have been investigated utilizing a VLS process, chemical synthesis, and metal organic chemical vapor deposition (MOCVD) (Morales and Lieber 1998; Jung and Ahn 2000).

Aluminum oxide is technologically an important material and is usually used as a catalyst support due to its thermochemical stability in various environments and media. It is well known that Al_2O_3 is one of the most thermodynamically stable oxides. The use of Al_2O_3 polycrystalline fibers and whiskers (short single crystals) as strengtheners in high-temperature compositions is of great interest owing to their high elastic modulus and their thermal and chemical stability (Peng et al. 2002). However, many reports have been published about the vapor growth of aluminum nitride nanostructures where aluminum oxide has been detected as an impurity. Few reports have been published about the vapor growth of aluminum oxide nanostructures starting from aluminum metal as a precursor with and without a catalyst and in the presence of foreign metals (Peng et al. 2002). This might be due to the presence of a coherent oxide layer that is naturally formed on the surface of Al particles. Moreover, the low melting point of Al (660 °C) which is less than the temperature required for complete metal oxidation results in the coalescence of Al grains during the oxidation process. These two reasons can prevent oxygen flow to the particle's core and consequently lead to incomplete oxidation. Many research groups have reported the formation of an AlN phase along with an impurity of Al_2O_3 by the reaction of aluminum sulfide with ammonia gas through solid–gas reactions (Zheng et al. 2002). The aluminum oxide formation was derived from the reaction of Al_2S_3 with air during sample preparation. The reaction of Al with N_2 at 4 l/min flow rate in presence of KCl yielded about 90% pure AlN powder with impurities of Al_2O_3, AlON and KCl as reported by other authors (Qiu et al. 2003).

In this article, we report on the vapor growth of ZnO nanobelts and Al_2O_3 nanoribbons. The crystal structural and morphological characteristics of these nanostructures are investigated. Moreover, the catalytic oxidation of CO gas over ZnO and Al_2O_3 nanostructures with and without metal loading is also investigated.

Experimental

Materials and synthesis

In a series of experiments, Zn metal granules (Zn granules, 99.9%, <800 μm, Merck) were inserted in a graphite holder and thermally evaporated in a quartz tube of 120 cm length and 2.8 cm inner diameter at temperature of 950 °C. The quartz tube was mounted inside a high-temperature split-type tube furnace (Type 79300 Thermolyne) which then evacuated to a base pressure of about 1.5×10^{-1} Torr. The furnace was then heated up with a heating rate of 80 °C min^{-1} under controlled atmosphere and controlled pressure. Pure oxygen (99.99%) was introduced to quartz tube in a counter direction to the vacuum and the pressure was controlled at 200 Torr by controlling the main vacuum valve. After the desired temperature was reached, the reaction was carried out for 15 min. Then the oxygen flow stopped and the furnace was turned off and left to cool down to room temperature under vacuum. The set-up of the synthesis system is shown in Fig. 1.

For aluminum oxide synthesis, aluminum metal (Al, Reagent plus powder 99%, particle size <75 μm, Sigma-Aldrich) and ammonium chloride (NH_4Cl, +99.5%, Sigma-Aldrich) were mixed in a proper ratio (3:1) and introduced into the graphite holder. The furnace temperature was increased up to 1150 °C after evacuating the quartz tube to a base pressure of $\sim 1.5 \times 10^{-1}$ Torr. The oxygen gas valve was opened and the oxygen flow was kept for 15 min at a pressure of 300 Torr. When the reaction process finished, the oxygen gas flow was stopped and the furnace was turned off whereas the sample was left to cool down under vacuum until the sample reached room temperature.

Metal loadings on the zinc and aluminum oxide nanostructures were carried out by reduction of corresponding metal precursors (metal nitrates, $M_x(NO_3)_y$; M = Ni; Co; Cu; Pd or metal chloride, $HMCl_4$; M = Au). An appropriate amount of the metal precursors' aqueous solution was added to a suspension of ZnO or Al_2O_3 support. The solution was then heated up in a conventional microwave furnace for 60 s. Next hydrazine hydrate was added as a reducing agent and the pH of the solution was adjusted to 9–11 by the dropwise addition of NaOH while stirring for 15 min. After stirring the solution, it was heated in a microwave oven. The microwave power was typically 650 W and operated in 40 s cycles. The resulting deposits were washed with distilled water and ethanol and left to dry.

Tools and characterization

The resulting products were collected for physico-chemical characterization. Phase identifications were performed using X-ray diffractometer (XRD; X'Pert Philips Materials Research System) with Cu–K_α

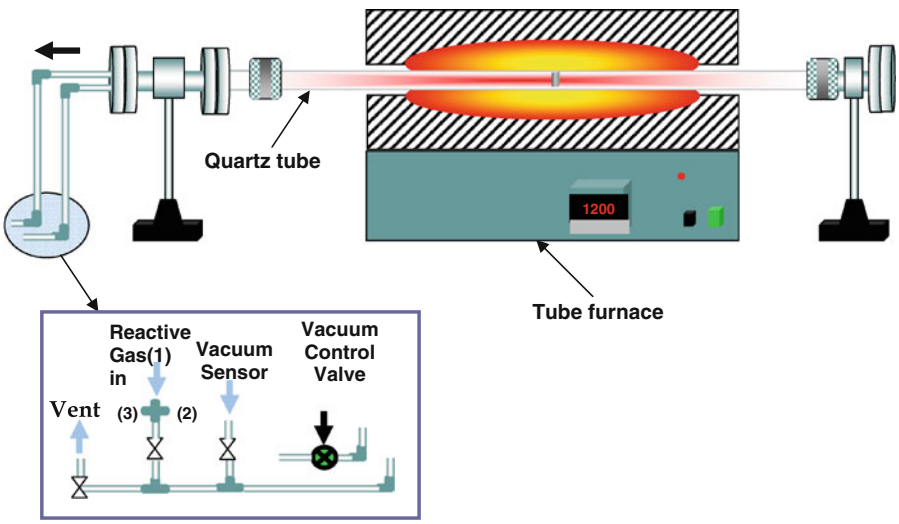

Fig. 1 Schematic representation of vapor growth of ZnO and Al_2O_3 nanostructures system set-up

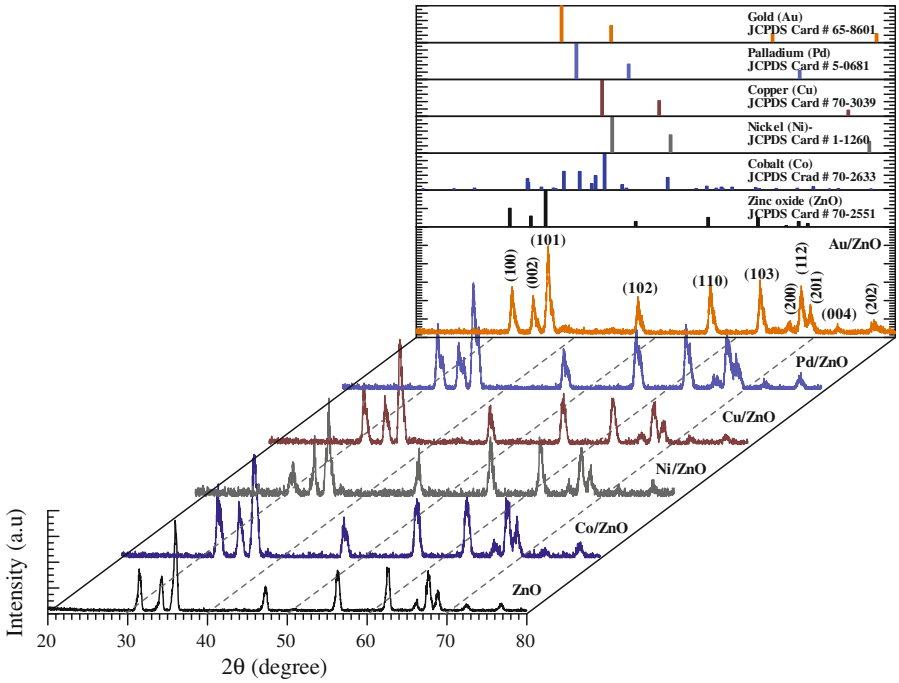

Fig. 2 XRD patterns of ZnO tetrapods (nanobelts) with and without metal loadings. The stick patterns of the corresponding materials are also shown for comparison

radiation ($\lambda = 1.5406$ Å) under an accelerating voltage of 45 kV and electric current of 40 mA in the 2θ range from 20°–80°. The morphologies and structures of the as-deposited products and after metal loadings were investigated by transmission electron microscopy (TEM; JEOL JEM-1230) operating at 120 kV.

Catalytic performance

The catalytic oxidation of CO gas was performed to evaluate the efficiency of the prepared materials as catalysts. About 10 mg of powder sample with and without metal loadings was introduced into a quartz tube which was mounted horizontally inside a programmable tube furnace (Thermolyne 21100) where the sample temperature was measured independently by a thermocouple placed about 1 mm apart from the sample. The feed gas mixture was $CO/O_2/He$. The composition of the gas mixture was 3.4 wt% CO and 20 wt% O_2, respectively, in He gas. The total flow rate of the gas mixture was controlled at a rate of 100 sccm via a mass flow controller (MKS digital flowmeter). Monitoring of the CO gas concentration was performed using an infrared gas analyzer (ACS, Automated Custom Systems, Inc.).

Results and discussion

Crystal structure

The zinc oxide products deposit as a white powder on the lower temperature part of the inner wall of the quartz tube near to the target and counter to the oxygen flow direction whereas aluminum oxide products deposit as a grayish white powder inside the sample holder. Figures 2 and 3 show the XRD patterns of the as-grown products of zinc oxide and aluminum oxide nanostructures, respectively. In general, the peaks are broad with low intensity. This might be due to the small particle size of the grown nanostructures. The figure displays the phase composition and purity of each product. The stick diffraction patterns of ZnO (JCPDS card # 70-2551), Al_2O_3 (JCPDS card # 16-0394), α-Al_2O_3 (JCPDS card # 81-226), Co (JCPDS card # 70-2633), Ni (JCPDS card # 1-1260), Cu (JCPDS card # 70-3039), Pd (JCPDS card # 5-0681), and Au (JCPDS card # 65-8601) are also shown there for comparison. All the diffraction peaks from zinc oxide samples are ascribed to the hexagonal würtzite crystal structure of ZnO phase (Fig. 2). Whereas the diffraction peaks from aluminum oxide

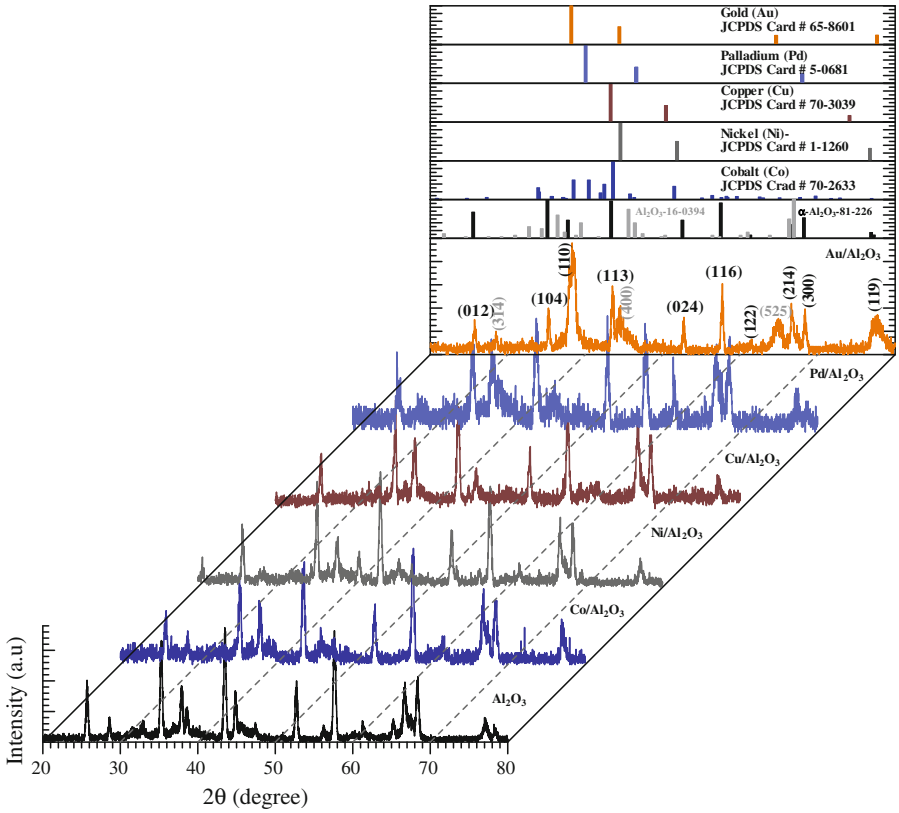

Fig. 3 XRD patterns of Al_2O_3 nanoribbons with and without metal loadings. The stick patterns of the corresponding materials are also shown for comparison

samples are ascribed to either Al_2O_3 or α-Al_2O_3 phases, respectively (Fig. 3). No other peaks corresponding to impurities such as Zn metal, Al metal, or other suboxides are observed in all samples. Moreover, the diffraction peaks from the loaded metal nanoparticles are not detected. This might be due to the fact that the amount (2 wt% upper limit based on the metal content of the starting precursors) and/or crystallinity of loaded metals are not enough to be clearly detected in the XRD patterns.

Morphology

The morphologies and structures of the as-grown and metal-loaded products are investigated by transmission electron microscopy (TEM). Figures 4 and 5 show the TEM images of the as-grown products. Figure 4a–c are the TEM images of ZnO tetrapods without metal loadings. They display a wave-like contrast implying the presence of strain which might be originating from the lattice mismatch or distortions (Lee et al. 2004). It is clear that in most cases the pods have almost uniform width and shapes over their entire length. They also end with needle shape-like tips. These needle-like tips are also observed for ZnO nanocrystals by other research groups (Fouad 2006). Typically the pods have lengths of several hundred nanometers ($\sim$400 to 500 nm) and widths of few nanometers ($\sim$10 to 30 nm). No metallic zinc particles are observed on the tip or at the end of the tetrapods as is also confirmed by XRD analyses. This reveals that the growth of ZnO tertrapods is not controlled by the VLS mechanism in which a metal particle is located at the growth front and acts as a heterogeneous catalyst for the growth of the tetrapod (Li et al. 2001). Moreover, it is likely that the process may be self-catalyzed where the tetrapods are grown by a small thin zinc layer present at the growth front. The small thin zinc layer is further oxidized, no longer present and cannot be detected (Morales and Lieber 1998). The driving forces for the formation of these nanostructures were found to be vapor density or

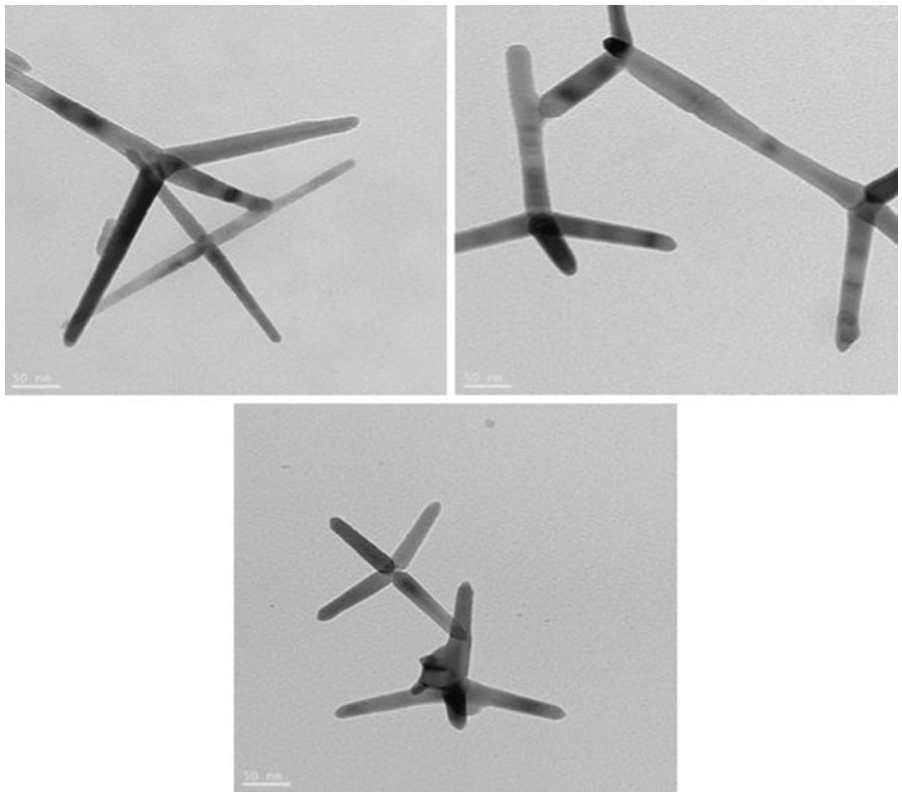

Fig. 4 TEM images of ZnO tetrapods (nanobelts) without metal loadings

supersaturation, temperature, pressure, and place of deposition from source materials (Fouad 2006; Fouad et al. 2008, 2010).

The TEM images of Al_2O_3 nanostructures are shown in Fig. 5. It is clear that the nanostructures form long nanoribbons as shown in Fig. 5. The ribbons have many folds and in some images show distorted complex structures. A single nanoribbon has an average width in the range of 20–30 nm and a length in the range of hundreds nanometers up to 1 μm. TEM images also show residual strain in the produced nanoforms. These nanostructures are believed to be grown without the contribution of catalyst particles since no hetero metal droplets are detected on the growth front which was always the case in previous study published by other groups (Morales and Lieber 1998).

The addition of NH_4Cl to Al metal powder results in the formation of an aluminum chloride through decomposition of ammonium chloride and formation of HCl gas (Eqs. 1–4). These reactions are thermodynamically favorable since the Gibbs free energies of formation are large negative values (Lide 2003).

$$NH_4Cl_{(s)} = NH_{3(g)} + HCl_{(g)} \quad \Delta G_{f1000K} = -93.2 \text{ kJ mol}^{-1} \tag{1}$$

$$Al_{(s)} + 3HCl_{(g)} = AlCl_{3(g)} + 3/2H_{2(g)} \quad \Delta G_{f1000K} = -326.4 \text{ kJ mol}^{-1} \tag{2}$$

$$2AlCl_{3(g)} + 3/2O_{2(g)} + 3H_{2(g)} = Al_2O_{3(s)} + 6HCl_{(g)} \quad \Delta G_{f1000K} = -929.5 \text{ kJ mol}^{-1} \tag{3}$$

The net proposed reaction is as follows:

$$NH_4Cl_{(s)} + 2Al_{(s)} + 3/2O_{2(g)} = Al_2O_{3(s)} + HCl_{(g)} + NH_{3(g)} \quad \Delta G_{f1000K} = -1489.1 \text{ kJ mol}^{-1} \tag{4}$$

The evolution of NH_3 and HCl gases due to the sublimation decomposition of NH_4Cl generates several pores which hinder the coalescence of the Al particles after melting and allows a better nitrogen flow into the cores of the grains. That mechanism promotes the chlorination process and consequently promotes the formation of aluminum oxide nanostructures.

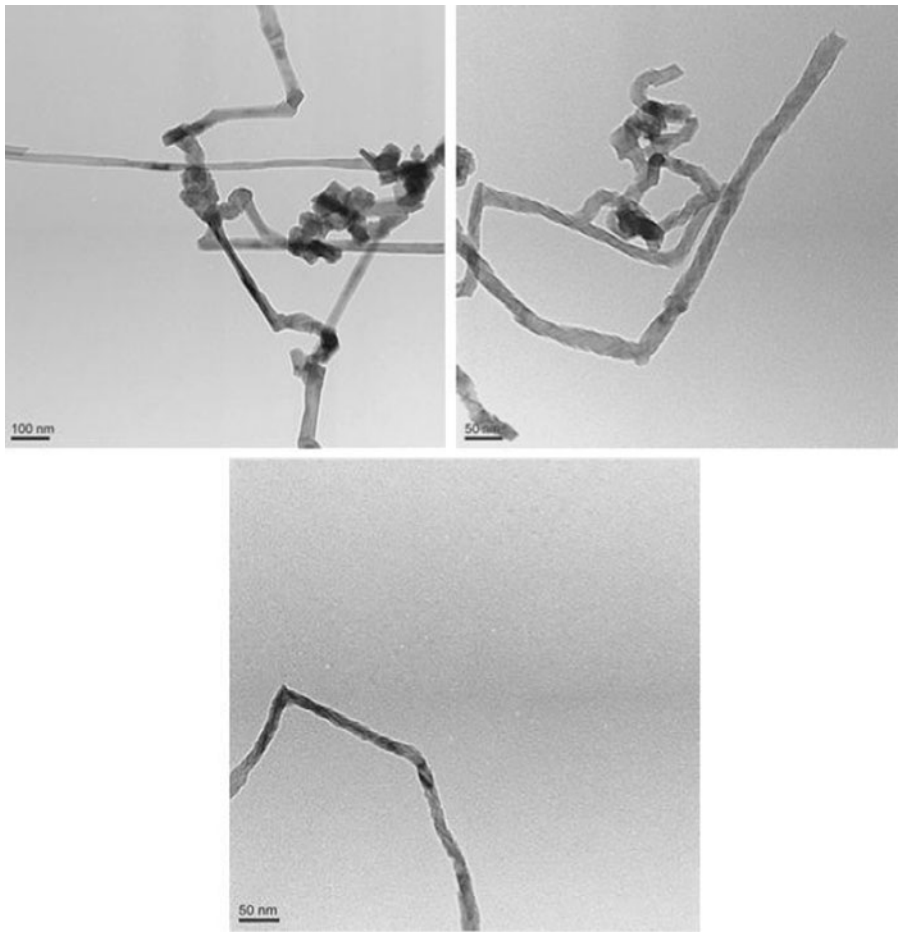

Fig. 5 TEM images of Al_2O_3 nanoribbons without metal loadings

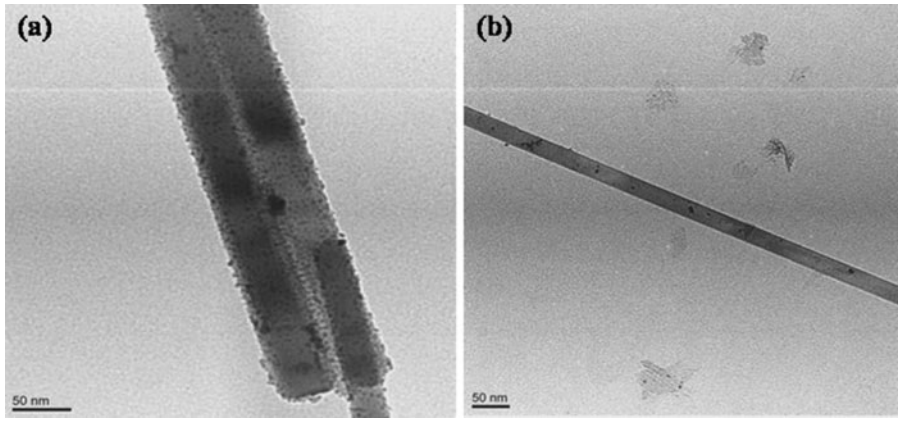

Fig. 6 TEM images of nanostructures with loaded Pd nanoparticle species. **a** Pd/ZnO nanobelts. **b** Pd/Al_2O_3 nanoribbons

TEM images of Pd-loaded ZnO and Al_2O_3 samples are shown in Fig. 6. It is clear that the metal nanoparticles are deposited on the nanostructures upon reduction of the corresponding Pd $(NO_3)_2$ in a microwave furnace using hydrazine hydrate as a reducing agent. It is obvious that nearly mono-, well-dispersed

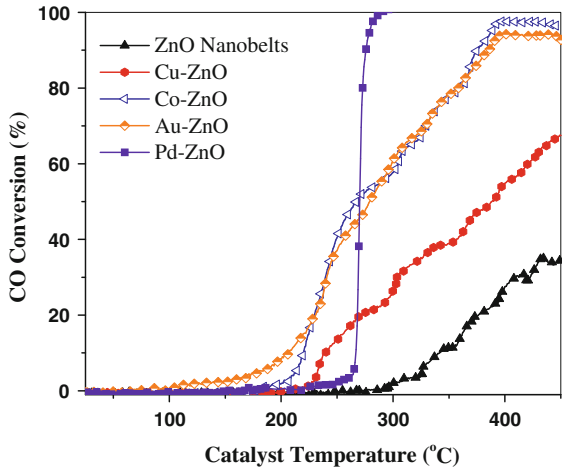

Fig. 7 Catalytic oxidation of CO gas over ZnO nanobelts

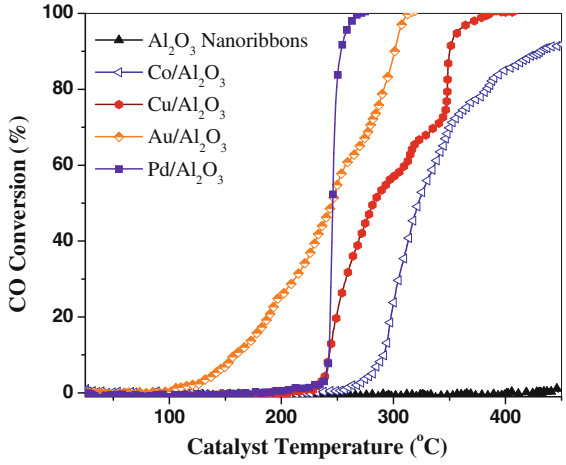

Fig. 8 Catalytic oxidation of CO gas over Al_2O_3 nanoribbons

very small Pd nanoparticles with an average size of 2–5 nm are formed.

Figures 7 and 8 compares the CO conversions over different 2 wt% metallic nanocatalysts supported on ZnO and Al_2O_3 prepared by the microwave irradiation method, respectively. The metal wt% was calculated from the metal content in the starting metal precursors. Therefore, these amounts should be regarded as an upper limit of the metal contents in the final supported catalysts.

It is clear that the Pd samples exhibit the highest activity with 100% conversions of CO to CO_2 at temperatures of 270 and 250 °C, respectively. The performance of these catalysts is significantly improved as the metal nanoparticles are loaded over the ZnO and Al_2O_3 nanostructures. It is also clear that the Pd-nanostructured catalysts show sharp conversion of CO to CO_2 whereas other metal-loaded catalysts (Cu, Co, and Au) show gradual conversions. The catalytic activities of the Pd/ZnO and Pd/Al_2O_3 nanocatalysts shown in Figs. 7 and 8 are considered comparable with the commonly investigated metal-loaded/ceria catalysts reported by other research groups (Mu et al. 2005; Kongkanand et al. 2006; Zhu et al. 2007). The catalytic activity increased in the order Cu < Co < Au < Pd metal-loaded nanostructures.

Conclusion

ZnO nanobelts in the form of tetrapods and Al_2O_3 nanoribbons have been grown from the vapor phase of the corresponding metals. The width of the belts and/or ribbons was in the range of 10–30 nm whereas the length was up to 1 μm. Metal loadings (Cu, Co, Au, and Pd) over the synthesized nanostructures were successfully deposited using the microwave irradiation method. Catalytic oxidation of CO over ZnO nanobelts and Al_2O_3 nanoribbons showed that the 2 wt% Pd nanoparticles (2–5 nm) loaded nanostructures had higher conversion efficiencies (100%) at 270 and 250 °C, respectively. These results are comparable to the results obtained using the commonly investigated ceria nanoparticle supports with higher metal loading contents.

Acknowledgments We thank the US-Egypt Joint Research Grant # ENV-09-003-279 for the support of this study. We also thank the National Science Foundation (OISE-0938520) for the support of the "US-Egypt Advanced Studies Institute on Nanomaterials and Nanocatalysis for Energy, Petrochemicals and Environmental Applications" which facilitated the completion of this study. We thank RAK CAM (Ras Al Khaimah Center for Advanced Materials, Ras Al Khaimah, UAE) for the Sheikh SAQR postdoctoral fellowship for Qilin Dai.

References

Aoki T, Hatanaka Y, Look DC (2000) ZnO diode fabricated by excimer-laser doping. Appl Phys Lett 76:3257–3258

Bai ZG, Yu DP, Zhang HZ, Ding Y, Gai XZ, Hang QL, Xiong GC, Feng SQ (1999) Nano-scale GeO2 wires synthesized by physical evaporation. Chem Phys Lett 303:311–314

Chen CC, Yeh CC (2000) Large-scale catalytic synthesis of crystalline gallium nitride nanowires. Adv Mater 12: 738–741

Choi YC, Kim WS, Park YS, Lee SM, Bae DJ, Lee YH, Park GS, Choi WB, Lee NS, Kim JM (2000) Catalytic growth of β-Ga_2O_3 nanowires by arc discharge. Adv Mater 12: 746–750

Chusuei CC, Lai X, Luo K, Goodman DW (2001) Modeling heterogeneous catalysts: metal clusters on metal oxide supports. Top Catal 14:71–83

Duan X, Lieber CM (2000) General synthesis of compound semiconductor nanowires. Adv Mater 12:298–302

Fouad OA (2006) Growth of zinc oxide nanorods, tetrapods, and nanobelts without catalyst. J Nanosci Nanotechnol 6: 2090–2094

Fouad OA, Glaspell G, El-Shall MS (2008) Growth and characterization of ZnO, SnO_2 and ZnO/SnO_2 nanostructures from the vapor phase. Top Catal 47:84–96

Fouad OA, Glaspell G, El-Shall MS (2010) Structural, optical and gas sensing properties of ZnO, SnO2 and ZtO nanostructures. NANO 5:185–194

Glaspell G, Fuoco L, El-Shall MS (2005) Microwave synthesis of supported Au and Pd nanoparticle catalysts for CO oxidation. J Phys Chem B 109:17350–17355

Glaspell G, Abdelsayed V, Saoud KM, El-Shall MS (2006a) Vapor-phase synthesis of metallic and intermetallic nanoparticles and nanowires: Magnetic and catalytic properties. Pure Appl Chem 78:1671–1689

Glaspell G, Hassan MA H, Elzatahry A, Fuoco L, Radwan NRE, El-Shall MS (2006b) nanocatalysis on tailored shape supports: Au and Pd nanoparticles supported on MgO nanocubes and ZnO nanobelts. J Phys Chem B 110:21387–21393

Henrich VE, Cox PA (1996) The surface science of metal oxides. Cambridge University Press, Cambridge

Holmes JD, Johnston KP, Doty RC, Korgel BA (2000) Control of thickness and orientation of solution-grown silicon nanowires. Science 287:1471–1473

Huang MH, Choudrey A, Yang P (2000) Ag nanowire formation within mesoporous silica. Chem Commun 12:1063–1064

Huang P, Wu F, Zhu B, Gao X, Zhu H, Yan T, Huang W, Wu S, Song D (2005) CeO_2 nanorods and gold nanocrystals supported on CeO_2 nanorods as catalyst. J Phys Chem B 109:19169–19174

Jung WS, Ahn SK (2000) Synthesis of aluminium nitride by the reaction of aluminium sulfide with ammonia. Mater Lett 43:53–56

Kongkanand A, Vingodgopal K, Kuwabata S, Kamat P (2006) Highly dispersed Pt catalysts on single-walled carbon nanotubes and their role in methanol oxidation. J Phys Chem B 110:16185–16188

Lee W, Jeong MC, Myoung JM (2004) Fabrication and application potential of ZnO nanowires grown on GaAs(002) substrates by metal–organic chemical vapour deposition. Nanotechnol 15:254

Li Y, Meng GW, Zhang LD, Phillipp F (2000) Ordered semiconductor ZnO nanowire arrays and their photoluminescence properties. Appl Phys Lett 76:2011

Li JY, Chen XL, Li H, He M, Qiao ZY (2001) Fabrication of zinc oxide nanorods. J Cryst Growth 233:5–7

Lide DR (ed) (2003) CRC handbook of chemistry and physics. CRC press LLC, London

Morales AM, Lieber CM (1998) A laser ablation method for the synthesis of crystalline semiconductor nanowires. Science 279:208–211

Moser WR (ed) (1996) Advanced catalysts and nanostructured materials. Academic Press, San Diego

Mu YY, Liang HP, Hu JS, Jiang L, Wan LJ (2005) Controllable Pt nanoparticle deposition on carbon nanotubes as an anode catalyst for direct methanol fuel cells. J Phys Chem B 109: 22212–22216

Narayanan R, El-Sayed MA (2004) Shape-dependent catalytic activity of platinum nanoparticles in colloidal solution. Nano Lett. 4:1343–1348

Narayanan R, El-Sayed MA (2005) Catalysis with transition metal nanoparticles in colloidal solution: nanoparticle shape dependence and stability. J Phys Chem B 09: 12663–12676

Peng XS, Zhang LD, Meng GW, Wang XF, Wang YW, Wang CZ, Wu GS (2002) Photoluminescence and infrared properties of α-Al2O3 nanowires and nanobelts. J Phys Chem B 106:11163–11167

Qiu Y, Gao L, Eur J (2003) Nitridation reaction of aluminum powder in flowing ammonia. Ceram Soc 23:2015–2022

Somorjai GA (1994) Introduction to surface chemistry and catalysis. Wiley Publishers, New York

Wu Y, Yang P (2000) Germanium nanowire growth via simple vapor transport. Chem Mater 12:605–607

Yazawa M, Koguchi M, Muto A, Ozawa M, Hiruma K (1992) Effect of one monolayer of surface gold atoms on the epitaxial growth of InAs nanowhiskers. Appl Phys Lett 61: 2051–2053

Ying JY, Tschope A (1996) in: Moser WR (ed) Advanced catalysts and nanostructured materials, Chapter 10. Academic press, San Diego pp 231–256

Zheng MJ, Zhang LD, Li GH, Shen WZ (2002) Fabrication and optical properties of large-scale uniform zinc oxide nanowire arrays by one-step electrochemical deposition technique. Chem Phys Lett 363:123–128

Zhu H, Qin Z, Shan W, Shen W, Wang J (2007) CO oxidation at low temperature over Pd supported on CeO2–TiO_2 composite oxide. Catal Today 126:382–386